Received: 28 February 2024 | Revised: 29 May 2024 | Accepted: 10 June 2024

DOI: 10.1002/alz.14120

Alzheimer's & Dementia®
THE JOURNAL OF THE ALZHEIMER'S ASSOCIATION

RESEARCH ARTICLE

Cellular prion protein acts as mediator of amyloid beta uptake by caveolin-1 causing cellular dysfunctions in vitro and in vivo

Angela da Silva Correia[1] | **Matthias Schmitz**[1] | **Anna-Lisa Fischer**[1] | **Susana da Silva Correia**[1] | **Franco L. Simonetti**[2] | **Gesine Saher**[3] | **Roberto Goya-Maldonado**[4] | **Amandeep Singh Arora**[5] | **Andre Fischer**[6,7] | **Tiago F. Outeiro**[8,9,10,11] | **Inga Zerr**[1]

[1]Department of Neurology, University Medical Center and the German Center for Neurodegenerative Diseases (DZNE), Georg-August University, Goettingen, Germany

[2]Fundación Instituto Leloir, Buenos Aires, Argentina

[3]Department of Neurogenetics, Max Planck Institute for Multidisciplinary Sciences, Goettingen, Germany

[4]Laboratory of Systems Neuroscience and Imaging in Psychiatry (SNIP-Lab), Department of Psychiatry and Psychotherapy, University Medical Center Goettingen (UMG), Goettingen, Germany

[5]Texas Therapeutics Institute, Brown Foundation Institute of Molecular Medicine, University of Texas Health Science Center at Houston, Houston, Texas, USA

[6]Department of Psychiatry and Psychotherapy, University Medical Center Goettingen, Goettingen, Germany

[7]Department for Systems Medicine and Epigenetics in Neurodegenerative Diseases, German Center for Neurodegenerative Diseases (DZNE) Goettingen, Goettingen, Germany

[8]Department of Experimental Neurodegeneration, Center for Nanoscale Microscopy and Molecular Physiology of the Brain, Center for Biostructural Imaging of Neurodegeneration, University Medical Center Goettingen, Goettingen, Germany

[9]Max Planck Institute for Multidisciplinary Sciences, Goettingen, Germany

[10]Translational and Clinical Research Institute, Faculty of Medical Sciences, Newcastle University, Newcastle, UK

[11]Scientific employee with an honorary contract at Deutsches Zentrum für Neurodegenerative Erkrankungen (DZNE), Goettingen, Germany

Correspondence
Matthias Schmitz, Department of Neurology, Georg-August University, Goettingen, Robert-Koch-Str. 40, 37075 Göttingen, Germany.
Email: matthias.schmitz@med.uni-goettingen.de

Funding information
Alzheimer Forschung Initiative, Grant/Award Numbers: 12851, 20026

Abstract

INTRODUCTION: Cellular prion protein (PrP^C) was implicated in amyloid beta (Aβ)-induced toxicity in Alzheimer's disease (AD), but the precise molecular mechanisms involved in this process are unclear.

METHODS: Double transgenic mice were generated by crossing Prnp knockout (KO) with 5xFAD mice, and light-sheet microscopy was used for whole brain tissue analyses. PrP^C-overexpressing cells were developed for in vitro studies, and microscopy was used to assess co-localization of proteins of interest. Surface-plasmon resonance (SPR) was used to investigate protein-binding characteristics.

RESULTS: In vivo, PrP^C levels correlated with reduced lifespan and cognitive and motor function, and its ablation disconnected behavior deficits from Aβ levels. Light-sheet microscopy showed that PrP^C influenced Aβ-plaque burden but not the distribution

Angela da Silva Correia and Matthias Schmitz contributed equally to this work.

of those plaques. Interestingly, caveolin-1 (Cav-1) KO neurons significantly reduced intracellular Aβ-oligomer (Aβo) uptake when compared to wild-type neurons.

DISCUSSION: The findings shed new light on the relevance of intracellular Aβo, suggesting that PrP^C and Cav-1 modulate intracellular Aβ levels and the Aβ-plaque load.

KEYWORDS
Alzheimer's disease, amyloid beta, caveolin, cellular prion protein

Highlights

- PrP^C expression adversely affects lifespan and behavior in 5xFAD mice.
- PrP^C increases Aβ1-40 and Aβ1-42 levels and Aβ-plaque load in 5xFAD mice.
- Cav-1 interacts with both PrP^C and Aβ peptides.
- Knocking out Cav-1 leads to a significant reduction in intracellular Aβ levels.

1 | BACKGROUND

Dementia is a syndrome in which there is a progressive deterioration of the cognitive function. Alzheimer's disease (AD) may contribute to 60% to 70% of dementia cases,[1] and the number of AD cases is expected to double by 2050.[1] Even though AD was described over 100 years ago, the exact pathological mechanisms are still incompletely understood, and there is no current cure or efficacious treatment. Since treatments for AD are essentially symptomatic, the development of disease-modifying approaches requires a better understanding of the molecular etiology of AD. A predominant theory, known as amyloid cascade hypothesis, posits that disease pathogenesis is associated with the progressive accumulation of amyloid beta (Aβ) peptide, derived from the cleavage of amyloid precursor protein (APP). The imbalance between Aβ production, aggregation, and clearance results in abnormal Aβ accumulation (reviewed by Crews and Masliah[2]). Aβ1-40 and Aβ1-42, containing 40 or 42 amino acid residues, respectively, are the dominant component of accumulated Aβ plaques. Aβ1-40 is frequently found, and Aβ1-42 is more toxic to neuronal cells.[3,4] Aβ accumulation in extracellular Aβ plaques was considered the primary culprit in AD. However, some research has shown evidence of intraneural Aβ in mice and humans,[5] thereby drawing attention to intracellular Aβ. Intraneuronal Aβ accumulation has been linked to the impairment of axonal transport and synaptic transmission, suggesting an important role in cognitive impairment associated with AD.[6,7] The precise mechanisms underlying AD remain unknown, but there is evidence that the neurotoxicity of Aβ oligomers (Aβo) is mediated by its interaction with synaptic receptors.[8] In this context, the cellular prion protein (PrP^C) was identified as a receptor for Aβo, modulating synaptic plasticity, suggesting that PrP^C is required to mediate the toxic effects of Aβo in AD.[9] A similar role was also shown in Parkinson's disease, where PrP^C was found to mediate alpha-synuclein-associated synaptic dysfunction.[10] PrP^C is highly expressed in the central nervous system[11] and is central to the pathogenesis of prion diseases.

In our study, we aimed to explore the role of PrP^C in AD using in vitro and in vivo experiments. In particular, we investigated the mechanisms of PrP^C-induced internalization of Aβ, identified proteins involved in the process, and assessed whether PrP^C deletion altered Aβ-related symptoms in vivo.

2 | MATERIALS AND METHODS

2.1 | Animals

The Central Animal Facility of Medical School Göttingen and the animal facility of the Max Planck Institute cared for the mice for Multidisciplinary Sciences, Göttingen. Animals were housed in constant conditions under 12/12 h light/dark cycle and temperature (21 to 22°C). Food and water were provided ad libitum. The strains used were 129B6 (mixed 129/Sv and C57BL/6 background) wild-type (WT) mice, 129B6/5xFAD mice express five AD-linked mutations: the K670N/M671L (Swedish), I716V (Florida), and V717I (London) mutations in human APP (695) and M146L and L286V mutations in PS1.[5] 129B6/$Prnp^{-/-}$ mice[12] lacking the neuronal cell-surface PrP^C protein. 129B6/5xFAD/$Prnp^{-/-}$ double transgenic mice exhibiting AD-linked mutations and the lack of cell-surface PrP^C protein. 129B6/$Prnp^{+/-}$ (cell-surface PrP^C heterozygous mice) were obtained crossing 129B6 with 129B6/$Prnp^{-/-}$ mice. 129B6/5xFAD/$Prnp^{+/-}$ carried AD-linked mutations and heterozygosity for PrP^C protein. Caveolin-1 (Cav-1) knockout (KO) mice.[13] Genotype was performed by polymerase reaction from the tail biopsy.

2.2 | Ethics

All animal procedures were approved by the Ethics Committee of the German Federal State of Niedersachsen and are in accordance with the European Union directive 2010/63/EU.

2.3 | Behavioral tests

Male mice were used for behavioral testing at 3, 9, 12, and 14 months old and were tested during the light cycle. Experimental mice were single caged 7 days prior to the start of the tests. During the test days, the animals were carried to the test room in their individual cages, 30 min prior to test start for adaptation to the conditions of the behavior testing room. The procedures were the same for all tested mice.

2.4 | Elevated plus maze

The apparatus used for the elevated plus maze test comprised two 60-cm-long open arms across from each other and perpendicular to two 60-cm-long closed arms with a center 10 × 10 cm platform. The closed arms had a 20-cm-high wall to enclose the arms, whereas the open arms had no walls. The entire apparatus was 50 cm above the floor and placed in an empty square (70 × 70 cm) to protect the fallen mice from escaping during the experiment. The mice were placed in the center of the platform and were allowed to explore the apparatus for 5 min. During this time, a video tracking system recorded their behavior (Video-Mot II, TSE, Bad Hamburg, Germany). After the test, the apparatus was cleaned with 70% ethanol and allowed to dry between sessions. The time spent in the open arms, closed arms, and central zone was analyzed.

2.5 | Rotarod

The rotarod apparatus consisted of a horizontal rotating bar rod that rotated about its long axis. A rotarod is designed to evaluate the fore and hind limb motor coordination, balance, physical condition, and motor planning of the tested animals. In the training phase, a mouse was placed on the rotarod at a constant speed of 5 rpm for a maximum duration of 280 s for five consecutive days. The testing day consisted of two trials with 5-min intertrial intervals, mice were placed on an accelerating rotarod from 4.0 to 40 rpm for 280 s, and the latency to fall was measured. Rotarod performance was assessed by evaluating the best trial out of two performed on the test day.

2.6 | Fear conditioning

Fear conditioning is a test of memory and learning in which mice learn to associate a context and cue with an unconditioned stimulus. The apparatus for the fear conditioning and context test was an acrylic square chamber (31.8 × 25.4 × 26.7 cm) with an electrifiable metal grid floor, a sound source, calibrated shock generator, and video system (Video Fear Conditioning (VFC) system, Med Associates, Fairfax, Vermont, USA). The conditioning step consisted in placing the mice in the chamber and allowing them to explore the chamber for 180 s with a background sound. After that, a tone was presented as a conditioned stimulus, and a 0.5-mA foot shock was given to the mice as an unconditioned stimulus during the last 2 s of the sound. The mice remained in the chamber for 30 s after the foot shock.

Twenty-four hours after the conditioning session, the mice were returned to the same conditioning chamber for 180 s for the contextual test in the absence of a tone and foot shock. The time that the mice froze was measured. The cued test was performed following the context test. In this test, the mice were placed in a different context, a smooth white floor that covered the metal grids and a curved white wall that covered the wall of the chamber. This provided a new context that was unrelated to the conditioning chamber. The mice were allowed to explore the chamber for 210 s, and in the last 180 s an auditory cue was presented that was given to the mice at the time of conditioning. The freezing behavior (absence of motion excluding respiration) was measured by video system (VFC system, Med Associates).

2.7 | Preparation of mice brain samples and protein extraction

The mice were sacrificed after a behavioral experiment via CO_2 asphyxiation, and then cervical dislocation was performed. Dissection was carried out on neuronal tissue and brains separated bilaterally into two equal parts. The cortex that covers the hippocampus was removed and used as a sample for molecular experiments. The cortex tissue was lysed by sonication in lysis buffer (150 mM NaCl, 50 mM Tris HCl [pH 7.5], 2 mM EDTA, and 1% Triton-x) containing protease and phosphatase inhibitor cocktail (Roche) for 30 min. Lysed tissue was

RESEARCH IN CONTEXT

1. **Systematic review**: We conducted a literature review on the molecular dynamics of PrP^C in AD using online databases. While previous studies acknowledged the significance of PrP^C in Aβo interactions, a comprehensive investigation of the molecular intricacies of the interaction and of the effects in AD pathology was lacking. The relevant literature has been thoroughly referenced.
2. **Interpretation**: The intricate link between PrP^C, Aβ peptides, and Cav-1 offers novel insights into AD pathogenesis. Elevated Aβ plaque load in critical brain regions and the correlation between Aβ levels and behavior underscore PrP^C's pivotal role in our model. The study introduces a potential molecular mechanism involving Cav-1 in PrP^C-mediated Aβ internalization.
3. **Future directions**: Future investigations should delve into downstream signaling pathways activated by PrP^C–Cav-1 interactions, validate findings in in vivo models and human samples, and explore therapeutic implications targeting these interactions for potential interventions in AD.

centrifuged at 13,000 rpm for 15 min at 4°C, and supernatant was obtained for further procedures.

2.8 | Immunoblotting

Protein concentration was determined using a Bicinchoninic Acid assay (Pierce™), and the same amount of protein from the different samples was separated on 10% to 15% SDS-PAGE gels and transferred on PVDF membranes. The membranes were blocked for 1 h in 5% non-fat milk in Tris-buffered saline with 0.1% Tween 20 (TBST) and incubated overnight at 4°C with the primary antibodies in blocking buffer (supplemental material). Subsequently, the membranes were washed in TBST at room temperature (RT). Then the secondary antibody (1:10000) in 5% non-fat milk in TBST was applied at RT for 1 h. Finally, after the final washing, the enzymatic reaction was performed using ECL solution and visualized with Molecular Imager ChemiDoc XRS+ with Image Lab Software (Bio-Rad). Densitometric values for each band intensity were determined using Image Lab 2.7.1 data analyzer software.

2.9 | Enzyme-linked immunosorbent assay (ELISA)

Aβ40 and Aβ42 from mouse cortex were quantified with ELISA Aβ1-40 (IBL International) and ELISA Aβ1-42 (IBL International), respectively. The quantification of PrP^C was obtained through prion protein (Prnp) (Cloud-Clone Corp.) ELISA. The ELISA procedures were performed according to supplier's recommendations.

2.10 | Aβ peptide preparation

The method followed to generate oligomeric Aβ was previously described.[14,15] Lyophilized synthetic human Aβ1-40 (Abcam) and Aβ1-42 (Abcam) were suspended in 1,1,1,3,3,3-Hexafluoro-2-Propanol (Sigma) to 1 mM solution, incubated for 2 h at RT, aliquoted, and posteriorly lyophilized via Speed-Vac. The Aβ films were stored at −80°C. Aβ films were resuspended in anhydrous dimethyl sulfoxide (DMSO) to a 5 mM final concentration and sonicated for 10 min in water bath. Aβ/DMSO was diluted in sterile phosphate buffer and then incubated overnight at 4°C to allow oligomerization.

2.11 | Cell culture and Aβ treatment

Human neuroblastoma cells wild type (SH-SY5Y WT) and human neuroblastoma cells stably expressing full-length human PrP^C (SH-SY5T PrP) were grown in Dulbecco's modified Eagle medium (DMEM; Biochrom, Berlin, Germany) supplemented with 10% heat-inactivated fetal calf serum (FCS; Biochrom), 1% penicillin/streptomycin (P/S; Biochrom), and 1% l-glutamine (Biochrom) at 37°C, 5% CO_2 supply, and 95% humidity. Then the cells were treated separately at a final concentration of 10 μM Aβ40 and Aβ42 for 24 h in DMM.

2.12 | Preparation of primary cortical neuronal cultures

For primary cortical neurons, the brains from P0 pups were collected. Briefly, the meninges were removed and the cortex tissue was digested in enzyme buffer (Hank's balanced salt solution [HBSS, Sigma-Aldrich] with 20-25 Papain units, 10 μg/mL DNAse, 400 mM Cysteine, 50 mM EDTA, and 1 M CaCl2) for 20 to 30 min at 37°C. Subsequently, cells were incubated at 37°C with plating medium (Neurobasal [Sigma-Aldrich], 100x Glutamax [Thermo Fisher Scientific], 10% FBS [Sigma-Aldrich], 0.2% Primocin [Thermo Fisher Scientific], and 50x B27 [Thermo Fisher Scientific]) for 5 min. Then the cells were washed twice in HBSS buffer (HBSS solution [Thermo Fisher Scientific], 1 M HEPES [Thermo Fisher Scientific], 100 mM pyruvic acid [Thermo Fisher Scientific], ddH2O [B. Braun], and 0.2% Primocin [Thermo Fisher Scientific]). The cells were resuspended in plating medium, counted, and plated on poly-L-ornithine and laminin-coated slide flasks (Sarstedt). The plating medium was replaced the following day with neuronal buffer (Neurobasal [Thermo Fisher Scientific], 100x Glutamax [Thermo Fisher Scientific], 50x B27 [Thermo Fisher Scientific], and 0.2% Primocin [Thermo Fisher Scientific]). Half of the medium was replaced with fresh medium every 3-4 days.

2.13 | Immunofluorescence

For immunofluorescence analysis, cells were cultured in x-well cell culture chambers, and the desired protocol was followed. Subsequently, the cells were fixated in freshly prepared 4% paraformaldehyd (PFA) for 10 min. After fixation, the cells were washed three times in phosphate buffered saline (PBS) and subsequently permeabilized in PBS + 0.2% Triton-X-100 for 10 min. Following permeabilization, the cells were blocked in phosphate buffered saline with 0.1% Tween (PBST) + 2% BSA for 30 min. After blocking, the cells were incubated with the primary antibody of interest (supplemental material) for 1 h at RT. Next, the cells were washed three times with PBS and incubated with their suitable fluorescent antibodies at RT for 1 h. After incubation, the cells were washed three times with PBS, and the chambers were sealed and observed under the microscope.

2.14 | Transmission electron microscopy

Transmission electron microscopy (TEM) was performed to examine the solutions with 300 μM oligomerized Aβ1-40 and Aβ1-42. A Formvar-coated copper EM grid was floated on 10 μL of sample followed by the addition of 10 μL of 0.25% glutaraldehyde. After 1 min, the grid was washed in three drops of water. For contrast, the grid was incubated with 2% aqueous uranyl acetate solution for 30 to 60 s. Excess uranyl acetate solution was removed by gently touching the grid vertically with a piece of filter paper. The negatively stained samples were imaged with TEM and the digital micrographs were obtained with an on-axis 2048*2048-CCD camera (TRS, Moorenweis, Germany).

2.15 | Surface-plasmon resonance measurements

Protein interaction analysis was conducted using a ProteOn XPR36 Protein Interaction Array system. To immobilize human recombinant PrP^C, a GLH sensor chip was utilized, resulting in a final immobilization level of 2200 response unit (RU). A ligand surface lacking any bound protein served as blank. Measurements were carried out at 25°C, and analytes were diluted in PBST. Aβ1-40, Aβ1-42, and Cav-1 were tested at concentrations of 15 µg/mL and 20 µg/mL. The signal obtained from the blank was subtracted from the protein-bound signal. The ProteOn analysis software utilized the Langmuir 1:1 interaction model to calculate the corresponding association and dissociation rate constants.

2.16 | Production of human recombinant PrP^C

The human recombinant PrP^C was purified following a previously described method.[16]

Briefly, the pET41a (+) vectors containing the gene encoding human PrP^C 23-230 (Biocat) were introduced into *E. coli* Rosetta cells (DE3) (Merck Millipore). The transformed cells were then cultured on Luria-Bertani agar (LB) medium supplemented with kanamycin (50 µg/mL) and chloramphenicol (34 µg/mL) in Petri dishes. The cultures were incubated overnight at 37°C. A single colony from the transformed cells was selected and added to LB medium containing kanamycin (50 µg/mL) and chloramphenicol (34 µg/mL). The culture was then incubated at 37°C with shaking at 250 rpm for 6 h. After incubation, Overnight Express Auto-induction system 1 (Sigma-Aldrich) was added, and the cells were further incubated at 37°C with shaking at 250 rpm for 20 h. Following incubation, the cells were harvested by centrifugation, and the supernatant was discarded. To purify the inclusion bodies, the cell pellet was resuspended and homogenized using 1X Bug Buster Mix (Merck Millipore). The suspension was incubated at room temperature for 20 min, and then 0.1X Bug Buster Master Mix (Merck Millipore) was added. The mixture was centrifuged at 13,000 × *g* for 15 min at 4°C. The pellet containing the inclusion bodies was dissolved in a solution of 8 M guanidine (38 g guanidine in 0.1 M NaPO4 at pH 8). The suspension was then incubated for 50 min at RT on a rotating mixer. After the incubation, the mixture was centrifuged at 13,000 × *g* for 5 min at 4°C to separate the soluble fraction from the insoluble components. The collected supernatant was combined with equilibrated Ni-NTA beads in denaturing buffer (6 M GdnHCl, 0.1 M $NaPO_4$ at pH 8) and incubated for 40 min. Following the incubation period, the Ni-NTA beads were loaded into an Äkta #XK16 column for purification. The tubes with the eluted proteins were collected from the largest UV 280 peak from the fast protein liquid chromatography (FPLC) and submitted to dialysis.

2.17 | Preparation of mice samples for 3D-analysis

Mice were anesthetized i.p. using a combination of ketamine (100 mg/kg) + medetomidine (1 mg/kg). The adequacy of anesthesia was assessed by tail and toe pinch responses. Subsequently, the skin and the diaphragm were opened to expose the chest cavity and the heart. A needle was inserted into the left ventricle, and a small cut was made in the right atrium. PBS + 1% heparin was pumped into the heart for 3 min at a rate of 4 mL/min, followed by 4% PFA solution for 5 min. Next, the brain was collected and placed in 4% PFA at 4°C overnight. On the following day, the brains were washed in PBS and stored at 4°C.

2.18 | Tissue clearing and immune-labeling through iDISCO+ protocol

In this study, the iDISCO+ method was employed.[17,18] Briefly, the washed samples underwent dehydration using a series of methanol/H_2O solutions (ranging from 20% to 100%). Each solution was incubated with the sample for 1 h. Following dehydration, the samples were washed in 100% methanol for 1 h and then chilled at 4°C. Then the samples were incubated overnight with shaking at RT in a solution consisting of 66% dichloromethane (DCM) and 33% methanol. The next day, the samples were washed twice in 100% methanol at RT and then chilled at 4°C. The samples were bleached in 5% H_2O_2 in methanol overnight at 4°C. On the following day, the samples were rehydrated using a series of methanol/H_2O solutions (ranging from 100% to 0%). Each solution was incubated with the sample for 1 h. In the end, the samples were washed twice at RT in PTx.2 (supplemental material). After the methanol treatments, the samples were subjected to immunolabeling. First they were incubated in permeabilization solution for 2 days at 37°C and then transferred to blocking buffer and incubated for another 2 days at 37°C. The primary antibody was diluted in PTwH/5% DMSO/3% donkey serum (supplemental material) and incubated with the samples for 5 days at 37°C, and then the samples were washed four to five times in PTwH for 1 day. The secondary antibody was diluted in PTwH/3% donkey serum and incubated with the samples for 5 days at 37°C. In the end, the samples were washed four to five times in PTwH for 1 day. Following immunolabeling, clearance was achieved through a series of methanol/H_2O (ranging from 20% to 100%), and each solution was incubated with the sample for 1 h. Subsequently, they were incubated in 66% DCM/33% methanol at RT with shaking for 3 h. Next, the samples were washed twice in 100% DCM for 15 min with shaking. Finally, the samples were immersed in dibenzyl ether (DBE) and stored in the darkness until imaging. The brain hemispheres were horizontally imaged using LaVision Ultramicroscope II and Imspector Microscope controller software.

2.19 | Light-sheet image analysis (QUINT)

The images acquired from the light-sheet microscope were preprocessed, registered, and analyzed using the QUINT workflow.[19] In summary, ImageJ software was utilized to convert images to the desired formats. The spatial registration of the mouse brains was performed using QuickNII with Allen Mouse Brain Atlas version 3 2017

reference atlas. Subsequently, the images were processed with VisuAlign for fine-tunning of the images registered in QuickNII. Ilastik software was used for pixel classification of the images. The spatial analysis was performed using Nutil software.

2.20 | Statistical analysis

Statistical analyses were performed using GraphPad Prism 10 software. For normally distributed data, a *t* test was employed. The lifespan of the mice was analyzed using a Mantel-Cox test and Gehan–Breslow–Wilcoxon test. Significant results were accepted as $^{*}p < .05$, $^{**}p < .01$, and $^{***}p < .001$. Pearson's correlation analysis was performed to analyze the correlation between variables of interest.

3 | RESULTS

3.1 | Expression of PrP^{C} and Aβ in double transgenic mice

We used western blot analysis of APP and PrP^{C} followed by densitometric quantification of APP were performed to confirm the genotype of different mouse lines used in this study: WT, 5xFADPrnp^{+}/$^{+}$, Prnp^{-}/$^{+}$, 5xFADPrnp^{-}/$^{+}$, Prnp^{-}/$^{-}$, and 5xFADPrnp^{-}/$^{-}$ (Figure S1A,B). To assess the levels of PrP^{C}, we utilized ELISA testing on mouse brain homogenates (Figure S1C-E). ELISA quantification revealed no difference between 5xFAD and WT mice and no correlation between PrP^{C} levels and aging in 5xFAD mice (Figure S1D,E). The Aβ1-40 and Aβ1-42 ELISAs were conducted on mouse brain homogenates to investigate the relationship between age and Aβ accumulation in different mouse lines (Figure 1A,B). A positive correlation was found between Aβ1-40 and Aβ1-42 levels and aging in the three different mouse lines. Next, we compared the levels of Aβ1-40 and Aβ1-42 in 5xFADPrnp^{+}/$^{+}$, 5xFADPrnp^{-}/$^{+}$, and 5xFADPrnp^{-}/$^{-}$ mice at 9 months of age (Figure 1C). Statistical analyses revealed a significant decrease of Aβ1-40 in 5xFADPrnp^{-}/$^{-}$ compared to 5xFADPrnp^{+}/$^{+}$ mice. No significant differences were found in Aβ1-40 levels when comparing 5xFADPrnp^{+}/$^{+}$ with 5xFADPrnp^{-}/$^{+}$ or 5xFADPrnp^{-}/$^{+}$ with 5xFADPrnp^{-}/$^{-}$. Similarly, the statistical analyses of Aβ1-42 demonstrated a significant decrease in 5xFADPrnp^{-}/$^{-}$ compared to both 5xFADPrnp^{+}/$^{+}$ and 5xFADPrnp^{-}/$^{+}$. There was no statistical difference in Aβ1-42 levels between 5xFADPrnp^{+}/$^{+}$ and 5xFADPrnp^{-}/$^{+}$.

3.2 | PrP^{C} modulation alters lifespan and behavior in 5xFAD mice

Examining the impact of PrP^{C} in the lifespan of 5xFAD mice (Figure 2A,B), we found a significant reduction in median lifespan for 5xFADPrnp^{+}/$^{+}$ (57% decrease) compared to WT. Similarly, 5xFADPrnp^{-}/$^{+}$ exhibited a 35% decrease in median lifespan compared to Prnp^{-}/$^{+}$ mice, and 5xFADPrnp^{-}/$^{-}$ showed a 16% decrease compared to Prnp^{-}/$^{-}$ mice (Figure 2A,B).

The open field test (Figure 2C) demonstrated a significant decrease in locomotor activity in 5xFADPrnp^{+}/$^{+}$ mice at 9 months compared to WT (Figure 2, C1). Similarly, 5xFADPrnp^{-}/$^{+}$ mice displayed a significant decrease at 12 months compared to Prnp^{-}/$^{+}$ mice (Figure 2, C2). No significant differences were observed in locomotor activity for Prnp^{-}/$^{-}$ and 5xFADPrnp^{-}/$^{-}$ mice (Figure 2, C3) across the various ages (3, 9, 12, and 14 months).

Rotarod testing revealed a decline in motor performance in 5xFADPrnp^{+}/$^{+}$ mice at 9 months compared to WT (Figure 2, D1) and in 5xFADPrnp^{-}/$^{+}$ mice at 12 months compared to Prnp^{-}/$^{+}$ mice (Figure 2, D2). No significant differences were observed in motor performance between Prnp^{-}/$^{-}$ and 5xFADPrnp^{-}/$^{-}$ mice (Figure 2, D3) from 3 to 12 months. Comparing the performance between the two groups at 14 months of age, we observed a significant decline of the motor function in 5xFADPrnp^{-}/$^{-}$ in comparison with Prnp^{-}/$^{-}$.

Using the elevated plus maze for assessing anxiety-related behavior showed a decrease in anxiety for 5xFADPrnp^{+}/$^{+}$ mice at 9 months compared to WT (Figure 2, E1) and for 5xFADPrnp^{-}/$^{+}$ mice at 12 months compared to Prnp^{-}/$^{+}$ mice (Figure 2, E2). 5xFADPrnp^{-}/$^{-}$ mice (Figure 2, E3) exhibited a decrease in anxiety at 12 and 14 months compared to Prnp^{-}/$^{-}$.

In the fear conditioning test, 5xFADPrnp^{+}/$^{+}$ mice displayed a decline of associative learning at 9 months compared to WT (Figure 2, F1), and 5xFADPrnp^{-}/$^{+}$ mice exhibited impaired associative learning at 9 and 12 months compared to Prnp^{-}/$^{+}$ mice (Figure 2, F2). Significant differences between 5xFADPrnp^{-}/$^{-}$ and Prnp^{-}/$^{-}$ emerged at 12 and 14 months, with 5xFADPrnp^{-}/$^{-}$ mice showing impaired associative learning (Figure 2, F3).

3.3 | Correlation between Aβ1-40 and Aβ1-42 levels and behavior in 5xFAD transgenic mice

Here, we explored the potential correlation between Aβ1-40 and Aβ1-42 levels and behavioral performance in transgenic mice. The study involved a range of behavioral tests, followed by the analysis of brain homogenates using ELISAs to quantify Aβ levels. In particular, we investigated the potential link between Aβ1-40 and Aβ1-42 levels and locomotor activity in mice of various genetic backgrounds (5xFADPrnp^{+}/$^{+}$, 5xFADPrnp^{-}/$^{+}$, and 5xFADPrnp^{-}/$^{-}$) using the open field test (Figure 3A,B). Notably, in 5xFADPrnp^{+}/$^{+}$ mice, there was no significant correlation between Aβ1-40 or Aβ1-42 levels and locomotor activity. Similar trends were observed in 5xFADPrnp^{-}/$^{+}$ and 5xFADPrnp^{-}/$^{-}$ mice, suggesting no substantive connection between Aβ levels and locomotor performance in the open field test.

To assess motor performance, we utilized the rotarod test. Significant negative correlations were observed between Aβ1-40 levels and motor performance in all three mouse models (Figure 3C), indicating that higher Aβ1-40 levels were linked to impaired motor skills.

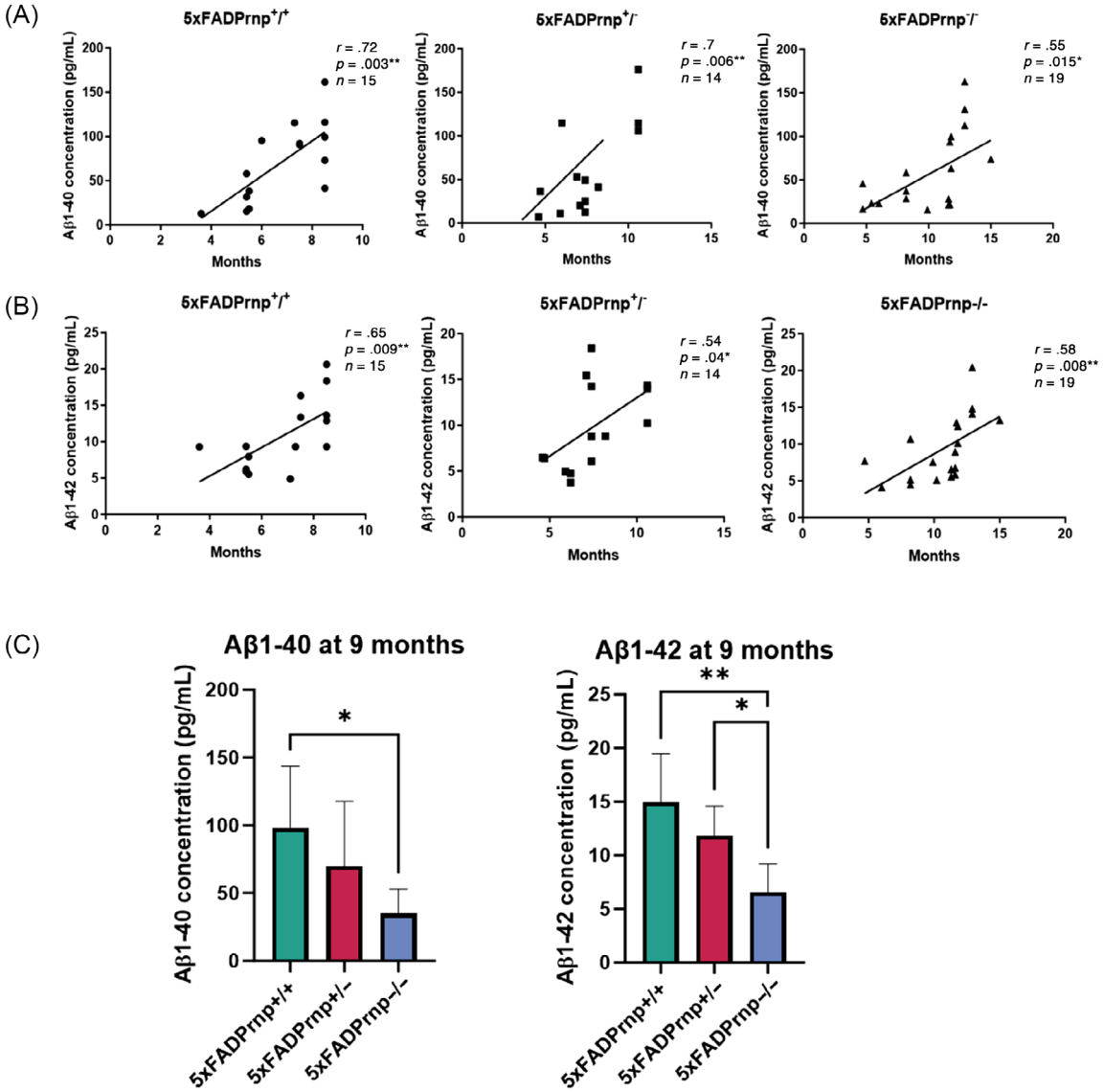

FIGURE 1 Correlation of amyloid-beta levels with aging. (A, B) In 5xFADPrnp$^{+/+}$ mice we observed a positive correlation for Aβ1-40 ($r = 0.72$, $p = .003$) and Aβ1-42 ($r = 0.65$, $p = .009$) with aging. For 5xFADPrnp$^{-/+}$ mice, a positive correlation was found for Aβ1-40 ($r = 0.7$, $p = .006$) and Aβ1-42 ($r = 0.54$, $p = .04$). The 5xFADPrnp$^{-/-}$ group displayed a positive correlation for Aβ1-40 ($r = 0.55$, $p = .015$) and Aβ1-42 ($r = 0.58$, $p = .008$). The p values indicate statistical significance in all cases. (C) Aβ1-40 and Aβ1-42 levels were measured in different mouse models. Aβ1-40 levels exhibited a statistically significant decrease in 5xFADPrnp$^{-/-}$ compared to 5xFADPrnp$^{+/+}$ mice (*$p = .03$). No statistically significant differences were observed in Aβ1-40 levels when comparing 5xFADPrnp$^{+/+}$ with 5xFADPrnp$^{-/+}$ mice or 5xFADPrnp$^{-/+}$ with 5xFADPrnp$^{-/-}$ mice. Analyses of Aβ1-42 levels revealed a significant decrease in 5xFADPrnp$^{-/-}$ compared to both 5xFADPrnp$^{+/+}$ (**$p = .007$) and 5xFADPrnp$^{-/+}$ mice (*$p = .02$). No significant differences were found in Aβ1-42 levels between 5xFADPrnp$^{+/+}$ and 5xFADPrnp$^{-/+}$ animals.

Similarly, Aβ1-42 levels (Figure 3D) in 5xFADPrnp$^{+/+}$ and 5xFADPrnp$^{-/+}$ mice showed significant negative correlations with motor performance. However, in 5xFADPrnp$^{-/-}$ mice, no significant correlation was found between Aβ1-42 levels and motor performance.

We also assessed anxiety-like behavior using the elevated plus maze test, examining correlations with Aβ1-40 and Aβ1-42 levels across the three mouse groups (Figure 3E,F). 5xFADPrnp$^{+/+}$ mice exhibited a significant negative correlation between Aβ1-40 and Aβ1-42 levels and anxiety, indicating that higher Aβ levels were associated with reduced anxiety-like behavior. A similar correlation was observed in 5xFADPrnp$^{-/+}$ for Aβ1-40 and Aβ1-42. In 5xFADPrnp$^{-/-}$ mice, no significant correlation was found between Aβ levels and anxiety.

Furthermore, we evaluated the correlations between Aβ1-40 and Aβ1-42 levels and associative learning. In 5xFADPrnp$^{+/+}$ mice, higher levels of both Aβ1-40 and Aβ1-42 were significantly correlated with impaired associative learning skills (Figure 3G,H). However, no significant correlations were found in 5xFADPrnp$^{-/+}$ and 5xFADPrnp$^{-/-}$ mice, indicating that Aβ levels did not substantially impact associative learning performance in these mouse models.

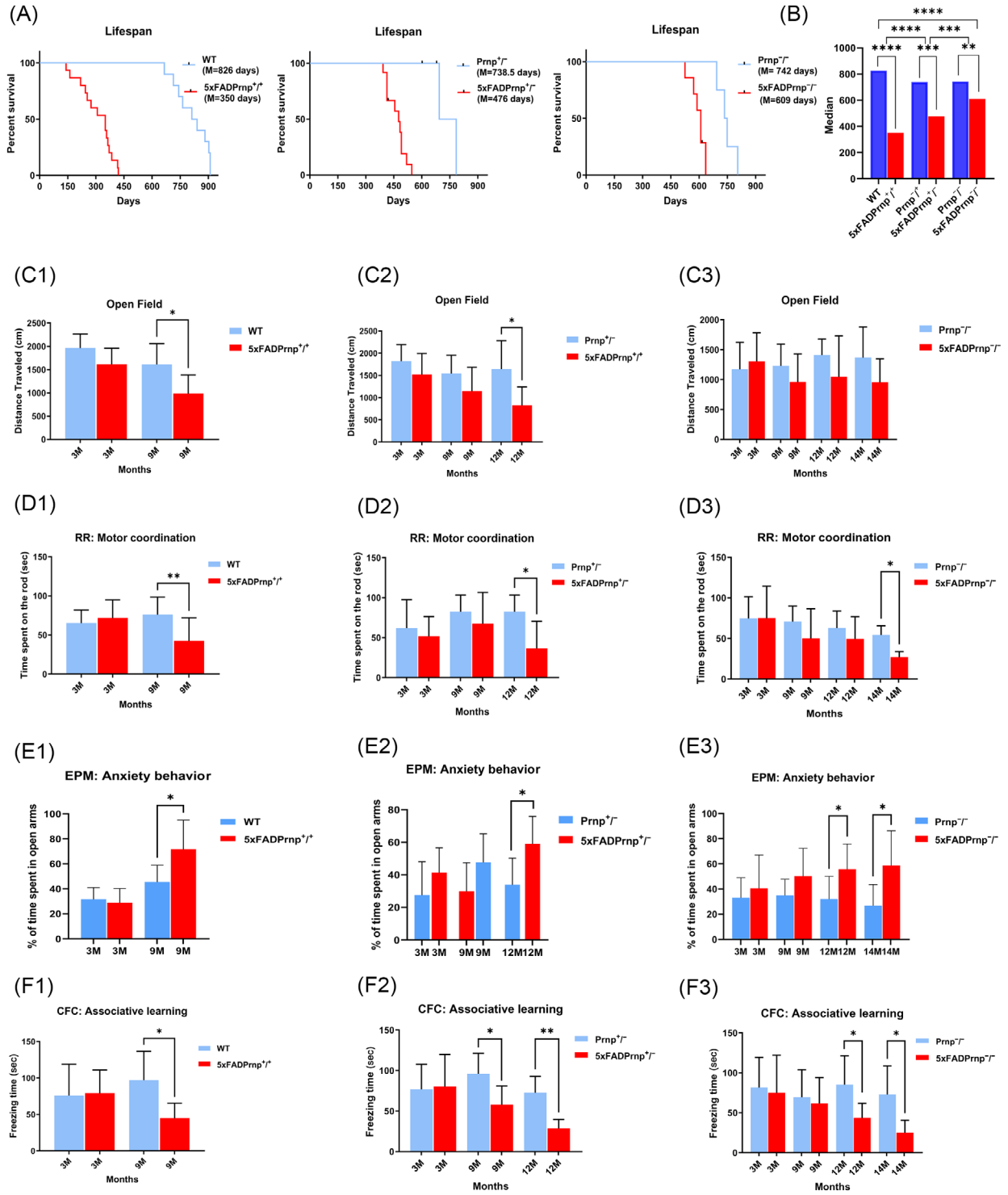

FIGURE 2 Influence of PrP level on the lifespan and mice behavior.(A) Comparison of lifespan between WT mice ($n = 10$) (M = 826 days) and 5xFADPrnp^{+}/$^{+}$ ($n = 15$) (M = 350 days), Prnp^{-}/$^{+}$ ($n = 5$) (M = 738 days), and 5xFADPrnp^{-}/$^{+}$ ($n = 12$) (M = 476 days) and between Prnp^{-}/$^{-}$ ($n = 4$) (M = 742 days) and 5xFADPrnp^{-}/$^{-}$ ($n = 7$) (M = 609 days). (B) Comparison of median lifespans. Statistical significance (****$p < .0001$) between WT and 5xFADPrnp^{+}/$^{+}$, (***$p = .0001$) between Prnp^{-}/$^{+}$ and 5xFADPrP^{-}/$^{+}$, and (**$p = .008$) between Prnp^{-}/$^{-}$ and 5xFADPrnp^{-}/$^{-}$ mice. The comparison between 5xFADPrnp^{+}/$^{+}$ and 5xFADPrnp^{-}/$^{+}$ presented a significance of $p < .0001$, of $p = .0001$ between 5xFADPrP^{-}/$^{+}$ and 5xFADPrnp^{-}/$^{-}$, and of $p < .0001$ between 5xFADPrnp^{+}/$^{+}$ and 5xFADPrnp^{-}/$^{-}$. (C) Distance traveled (centimeters) in open field test ($n = 6$). (C1) Comparison of distance traveled between WT and 5xFADPrnp^{+}/$^{+}$. At 9 months, 5xFADPrnp^{+}/$^{+}$ showed a significant reduction in distance traveled compared with WT mice (*$p = .04$). (C2) Comparison between Prnp^{-}/$^{+}$ and 5xFADPrnp^{-}/$^{+}$ mice. At 12 months of age, 5xFADPrnp^{-}/$^{+}$ mice exhibited a significant decrease in distance traveled compared to Prnp^{-}/$^{+}$ (*$p = .03$). (C3) Comparison between Prnp^{-}/$^{-}$ and 5xFADPrnp^{-}/$^{-}$. No significant differences in distance traveled were observed across all tested ages. (D) Motor function ($n = 6$). (D1) Motor function comparison: 5xFADPrnp^{+}/$^{+}$ mice showed significant (**$p = .004$) decline of motor function at 9 months. (D2) At 12 months 5xFADPrnp^{-}/$^{+}$ mice showed

3.4 | PrP^C modulation affects Aβ-plaque load in 5xFAD mice

In the investigation of 5xFADPrnp$^{+/+}$ mouse brains, distinctive patterns of Aβ-plaque distribution emerged across various regions (Figure 4, A1-9), revealing widespread deposition, particularly prominent in the cortex (Figure 4, A1), olfactory area (Figure 4, A4), and hippocampus (Figure 4, A3). The hypothalamus, thalamus, and mid-hind medulla also displayed significant Aβ-plaque loads, while regions such as fiber tracts, striatum, palladium, and the ventricular system exhibited comparatively lower plaque loads.

A parallel analysis of Aβ plaques in 5xFADPrnp$^{-/-}$ mouse brains revealed a widespread distribution (Figure 4, B1-9), with a predominant deposition in the cortex (Figure 4, B1), followed by the olfactory areas (Figure 4, B4) and hippocampus (Figure 4, B3). The hypothalamus and mid-hind medulla exhibited moderate plaque loads, while fiber tracts, ventricular system, thalamus, striatum, and pallidum showed lower Aβ-plaque loads compared to the previously described regions.

To identify potential differences in Aβ-plaque loads between 5xFADPrnp$^{+/+}$ and 5xFADPrnp$^{-/-}$ mice at 8 months of age, a statistical analysis was conducted (Figure 4C). Significant differences were observed in the cortex, where 5xFADPrnp$^{+/+}$ mice displayed a higher Aβ-plaque load than 5xFADPrnp$^{-/-}$. This trend persisted in the fiber tracts, hippocampus, olfactory areas, hypothalamus, mid-hind medulla, thalamus, and striatum and pallidum, although without statistical significance. Portions of the images captured with Ultramicroscope II and the three-dimensional (3D) reconstruction of the entire stack are available (Figure S2).

3.5 | Modulation PrP^C influences intracellular Aβ levels in SH-SY5Y^{PrPC} cells

SPR analysis was conducted to investigate the binding affinity between PrP^C and Aβo (oligomerization controlled in Figure S3), specifically, Aβ1-40 and Aβ1-42. The sensorgrams exhibited evident association and dissociation phases for both interactions (Figure 5A,B). The analysis revealed strong binding affinities with low equilibrium dissociation constants (KD) for both PrP^C–Aβ1-40 and PrP^C–Aβ1-42 interactions. The binding affinity of PrP^C with Aβ1-42 (KD = 1.13E-08 M) was found to be higher than that with Aβ1-40 (KD = 2.88E-08 M).

Subsequent confocal microscopy and Mander's coefficient analysis (Figure 5C-F) were used to investigate the colocalization of PrP^C with both Aβ1-40 and Aβ1-42 oligomers in cells with normal physiological PrP^C expression (SH-SY5Y^{WT}) and PrP^C-overexpressing cells, (SH-SY5Y^{PrPC}). The results revealed a significantly higher fluorescence signal for PrP^C, Aβ1-40, and Aβ1-42 in SH-SY5Y^{PrPC} in comparison with SH-SY5Y^{WT}. The Mander's coefficient analysis revealed similar levels of colocalization between PrP^C and Aβo in both cell lines.

Further validation was conducted using ELISAs to quantify the levels of intracellular Aβ1-40 and Aβ1-42 in both cell lines following treatment with Aβ1-40 and Aβ1-42 oligomers (Figure 5G,H). The ELISA results demonstrated a significant increase in the levels of both Aβ1-40 and Aβ1-42 in both cell lines after treatment, with significantly higher levels observed in the PrP^C-overexpressing cells compared with normal PrP^C expression cells.

3.6 | Caveolin-1 knockout reduces intracellular Aβ levels

To better understand the mechanism of PrP^C–Aβo internalization by cells, we searched for proteins closely colocated with PrP^C. PrP^C is enriched within caveolae, where Cav-1 serves as the predominant protein component, contributing to processes such as signaling transduction, lipid trafficking, and endocytosis. This prompted an exploration of potential association between PrP^C and Cav-1.

We employed the SPR to investigate the potential interaction between Cav-1 and PrP^C and found a significant and strong interaction between Cav-1 and PrP^C at both tested concentrations (10 and 20 µg/mL) (Figure 6A). The binding response displayed a concentration-dependent behavior, with a more pronounced interaction observed at higher PrP^C concentrations. Additionally, we wanted to investigate the potential interactions between Cav-1 and Aβ1-40 and Aβ1-42 (Figure 6B,C). Through SPR analysis, we quantitatively assessed the binding characteristics of these interactions by calculating the equilibrium KD. Our analysis revealed a specific and stable direct interaction between Cav-1 and Aβ1-40 at both concentrations tested (10 and 20 µg/mL). The sensorgrams obtained from these experiments displayed concentration-dependent binding, indicating a stronger interaction at higher concentrations of Aβ1-40. Similarly, the SPR analysis between Cav-1 and Aβ1-42 demonstrated a robust and specific interaction at both Aβ1-42 concentrations (10 and 20 µg/mL), also displaying concentration-dependent binding responses.

Following the SPR interaction confirmation of the interaction between Cav-1 with PrP^C, Aβ1-40, and Aβ1-42, we treated WT

significant decline of motor functions compared with Prnp$^{-/+}$ mice (*p = .01). (D3) At 14 months, 5xFADPrnp$^{-/-}$ mice performed significantly worse in comparison with Prnp$^{-/-}$ (*p = .02). (E) Anxiety behavior (n = 6). In (E1), at 9 months of age, 5xFADPrnp$^{+/+}$ mice showed a significant increase in time spent in open arms compared with WT mice (*p = .03). (E2) At 12 months of age, 5xFADPrnp$^{-/+}$ mice exhibited a significant increase of time spent in open arms in comparison with Prnp$^{-/+}$ (*p = .033). In (E3), significant increase of time spent in open arms in 5xFADPrnp$^{-/-}$ compared to Prnp$^{-/-}$ is observed at 12 (*p = .04) and 14 (*p = .02) months of age. (F) Freezing time on cued fear conditioning test (n = 6). (F1) 5xFADPrnp$^{+/+}$ displayed a decreased freezing time at 9 months of age in comparison with WT mice (*p = .04). (F2) At 9 and 12 months of age, 5xFADPrnp$^{-/+}$ exhibited a significant reduction in freezing time compared to Prnp$^{-/+}$, *p = .04 and **p = .004, respectively. In (F3), at 12 and 14 months of age, significant differences emerged between Prnp$^{-/-}$ and 5xFADPrnp$^{-/-}$ groups, with 5xFADPrnp$^{-/-}$ mice displaying a reduced freezing time, *p = .04 and *p = .03, respectively, compared to Prnp$^{-/-}$.

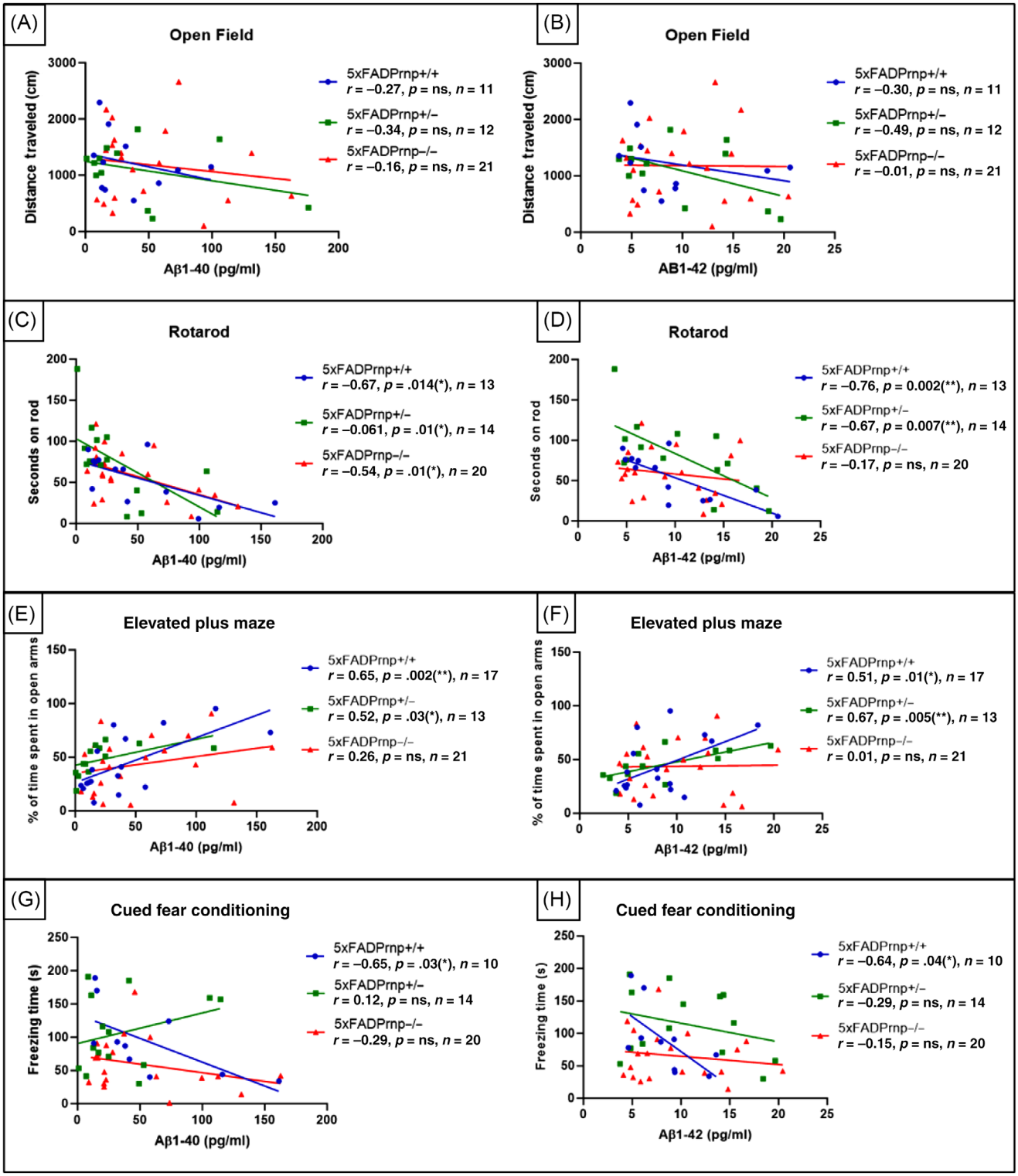

FIGURE 3 Amyloid beta (Aβ) levels and locomotor activity performance. Correlation analysis for (A) Aβ1-40 and (B) Aβ1-42 levels with distance traveled in open field test. No significant correlations were observed across 5xFADPrnp^{+}/$^{+}$, 5xFADPrnp^{-}/$^{+}$, and 5xFADPrnp^{-}/$^{-}$ mice. (C, D) Correlation analysis of Aβ levels with rotarod performance. The graphs showed a significant negative correlation between (C) Aβ1-40 and time on rod in 5xFADPrnp+/+ ($r = -0.67$, $^{*}p = .014$). Similarly, we observed a significant negative correlation between (D) Aβ1-42 and time on rod in 5xFADPrnp+/+ ($r = -0.76$, $^{**}p = .002$). In 5xFADPrnp-/+ mice, a significant negative correlation between (C) Aβ1-40 and time on rod ($r = -0.61$, $^{*}p = .01$) and between (D) Aβ1-42 and time on rod ($r = -0.67$, $^{**}p = 0.007$). Significant negative correlation between (C) Aβ1-40 and time on rod in 5xFADPrnp^{-}/$^{-}$ mice ($r = -0.54$, $^{*}p = .01$), indicating reduced time on rod with higher Aβ1-40 levels. No significant correlation between (D) Aβ1-42 and time on rod in 5xFADPrnp^{-}/$^{-}$ mice. (E, F) Correlation analysis of Aβ1-40 and Aβ1-42 levels with time spent on open arms. 5xFADPrnp^{+}/$^{+}$ showed a positive correlation between levels of (E) Aβ1-40 ($r = 0.65$, $^{*}p = .016$) and (F) Aβ1-42 ($r = 0.51$, $^{*}p = .01$) and time spent on open arms. Similarly, 5xFADPrnp^{-}/$^{+}$showed a positive correlation between levels of (E) Aβ1-40 ($r = 0.52$, $^{*}p = .03$) and (F) Aβ1-42 ($r = 0.67$, $^{**}p = .005$) and

and Cav-1 KO primary neurons with Aβ1-40 and Aβ1-42 oligomers overnight. Using Aβ1-40 and Aβ1-42 ELISAs, we quantified the levels of Aβ1-40 and Aβ1-42, respectively, in neuronal lysates (Figure 6D). The analyses revealed a significant reduction in Aβ1-40 (65% less) and Aβ1-42 (25% less) levels in Cav-1 KO neurons compared to WT neurons.

4 | DISCUSSION

4.1 | PrP^C modulates lifespan and behavior in 5xFAD mouse models: Aβ levels do not correlate with behavioral deficits in absence of PrP^C

The longevity results showed that elevated PrP^C levels, with 5xFAD mutations, correlated with reduced lifespan, indicating a PrP^C dose-dependent relationship. Studies on PrP^C in AD mouse models yield conflicting outcomes, with some suggesting PrP^C ablation does not prevent shortened lifespan (J20 and TgCRND8 mouse lines),[20,21] and others indicating normal survival in PrP^C-lacking mice (APPswe/PSen1dE9).[22,23] These discrepancies may arise from various factors, including experimental model background. Our findings diverge from existing reports as PrP^C ablation did not fully restore the lifespan but significantly increased it when compared to mice co-expressing PrP^C and 5XFAD mutations.

In the behavioral tests, the onset of the impairments was PrP^C dose-dependent, most pronounced in mice with higher PrP^C levels, and delayed in PrP^C-KO mice. While prior research on PrP^C ablation/blocking in AD mouse models predominantly emphasized learning and memory behaviors (J20 and APPswe/PSen1dE9[20,22,24–26]), our study covered a range of behavioral tests, offering a comprehensive understanding of PrP^C influence in 5xFAD mice. In APPswe/PSen1dE9 model, both PrP^C ablation and antibody blocking led to the reversal of cognitive deficits.[22,25] Conversely, in the J20 model, the ablation of PrP^C did not lead to the restoration of memory impairments.[20] Injection of synthetic Aβo revealed that mice lacking PrP^C were equally susceptible to Aβ-induced toxicity compared to mice expressing PrP^C.[26] The different outcomes could be attributed to distinctive characteristics of these mouse lines, including the pace and aggressiveness of AD-like pathology. 5xFAD mice exhibited aggressive Aβ pathology and severe cognitive deficits at an early age in comparison with J20 and APPswe/PSen1dE9 mice.[5] Another factor that may contribute to the differing findings is the single-time-point assessment, which may overlook the progressive nature of the disease. Thus, our assessments ranged from 3 to 14 months of age, allowing us to explore how PrP^C influenced the progression of AD-related pathology. Mice's motor condition evaluation is crucial, especially for tests like the Morris water maze (MWM) that require good motor function. Motor disabilities can yield misleading results, suggesting memory deficits when the primary issue is motor impairment. Hence, mice exhibiting exceptionally low locomotor activity were excluded for data reliability.

Analyses of Aβ levels suggested a link between Aβ1-40 and Aβ1-42 levels and impaired test performance in mice. This correlation, however, seems dependent on the presence of PrP^C's. In the absence of PrP^C, the correlation diminishes, with behavior impairments emerging later, not directly linked to Aβ levels. This underscores PrP^C's pivotal role in determining the association strength between Aβ levels and behavioral outcomes. The presence of specific Aβ conformations interacting with other receptors may exert substantial influence beyond Aβ levels in the absence of PrP^C. In the Tg2576 model, one study revealed no clear relationship between memory and insoluble Aβ levels when considering animals of different ages. This relationship was observed when the mice were separated into age-based subgroups.[27] Another study using an APP/PS1 model found no connection between the extent of Aβ pathology and cognitive deficits, suggesting Aβ levels may not serve as an indicator of memory decline.[28] A systematic review concluded that mice intentionally bred for higher Aβ levels did not exhibit significantly poorer cognitive performance compared to mice without elevated Aβ levels.[29] In humans, Aβ levels are frequently elevated in AD patients, yet they are not a reliable indicator of advancement and progression of AD among individuals.[30] One explanatory hypothesis suggests that cognitive impairments in AD may be linked to qualitative levels of Aβ rather than quantities of Aβ.[29]

4.2 | PrP^C expression correlates with elevated Aβ-plaque load in mice

Light-sheet microscopy analyses revealed a high Aβ-plaque load on mouse brains, suggesting a potential impact on cognitive and motor functions, consistent with observed behavioral impairments. Cortex Aβ plaques were significantly higher in 5xFADPrnp^{+}/$^{+}$ compared to 5xFADPrnp^{-}/$^{-}$ mice, with similar trends in other brain regions, albeit not at statistically significant levels. A generalized higher load of Aβ plaques in 5xFADPrnp^{+}/$^{+}$ mice suggests PrP^C's potential role in modulating Aβ-plaque load or influencing the spread of Aβ pathology in the brain. AD is characterized by Aβ accumulation in the brain, causing cognitive and behavioral impairments.[31] The cortex, olfactory area, and hippocampus are vital for cognitive processes such as memory, learning, voluntary movement, and sensory perception in mice.[32–36] In sHaPrP Tg7 mice expressing APPSwed+Ind with PrP^C overexpression, the cortex had a significantly higher load of Aβ plaques compared to mice with APPSwed+Ind mutations and normal physiological PrP^C levels.[37] In TgAD mice, increased Aβ-plaque levels were observed in

time spent on open arms. No significant correlation was found between (E) Aβ1-40 and (F) Aβ1-42 levels and the time spent on the open arms in and 5xFADPrnp^{-}/$^{-}$ mice. (G, H) Correlation analysis between Aβ levels and freezing time in cued fear conditioning test. 5xFADPrnp^{+}/$^{+}$ showed a negative correlation between (G) Aβ1-40 ($r = -0.65$, $^{*}p = .03$) and (H) Aβ1-42 ($r = -0.64$, $^{*}p = .04$) levels and freezing time. No significant correlations were found between (G) Aβ1-40 and (H) Aβ1-42 and freezing time in 5xFADPrnp^{-}/$^{+}$and 5xFADPrnp^{-}/$^{-}$ mice.

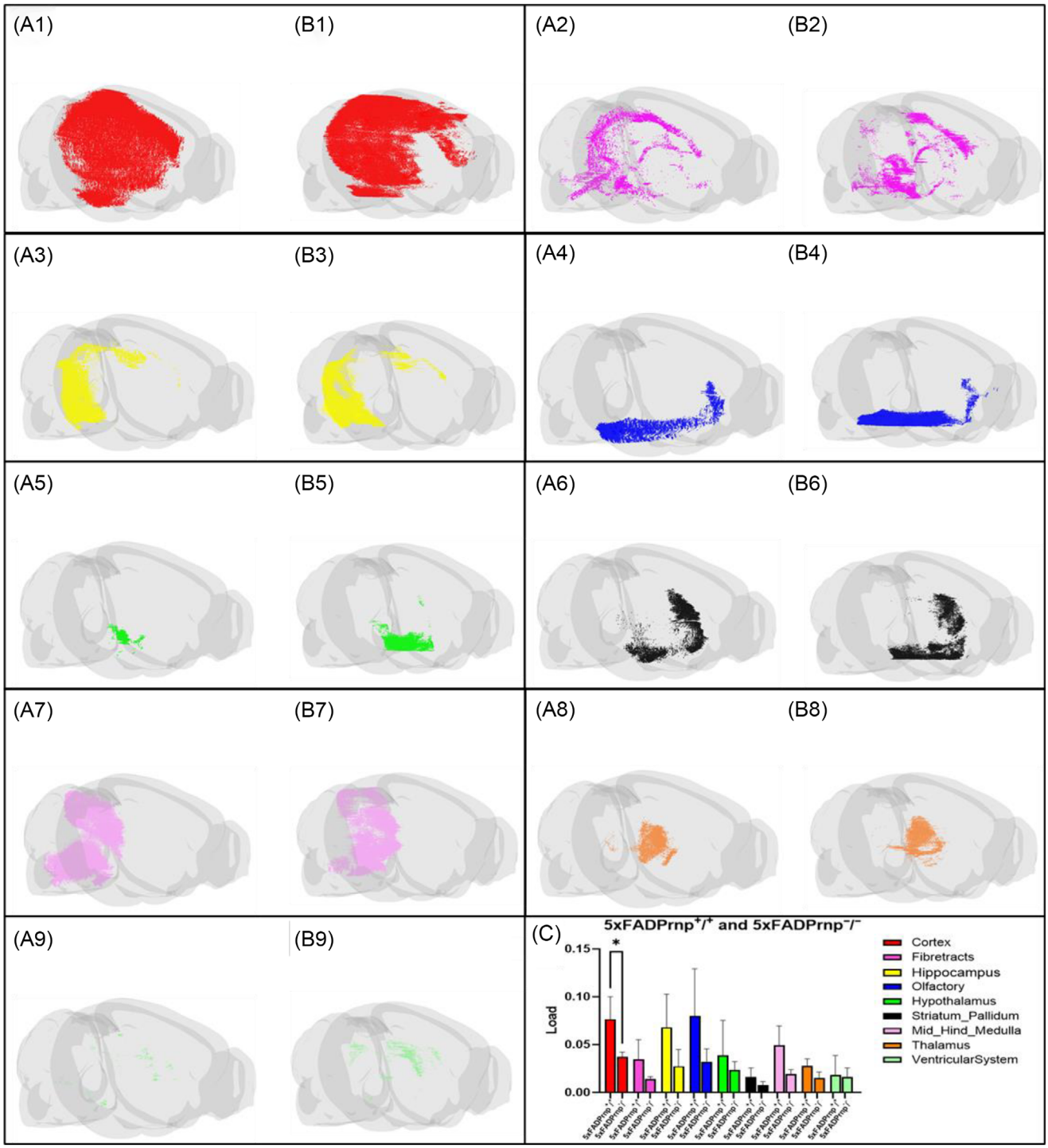

FIGURE 4 Three-dimensional imaging of Aβ-plaque distribution in various brain regions of 5xFADPrnp^{+}/$^{+}$ mice ($n = 3$). (A) Labeled regions: (A1) cortex, (A2) fiber tracts, (A3) hippocampus, (A4) olfactory areas, (A5) hypothalamus, (A6) striatum and palladium, (A7) mid-hind medulla, and (A8) ventricular system. (B) Three-dimensional imaging of Aβ-plaque distribution in various brain regions of 5xFADPrnp^{-}/$^{-}$ mice ($n = 3$). Labeled regions: (B1) cortex, (B2) fiber tracts, (B3) hippocampus, (B4) olfactory areas, (B5) hypothalamus, (B6) striatum and palladium, (B7) mid-hind medulla, and (B8) ventricular system. (C) Graph depicts comparative analysis of Aβ-plaque distribution in distinct brain regions between 5xFADPrnp^{+}/$^{+}$ and 5xFADPrnp^{-}/$^{-}$ mice ($n = 3$). In the cortex, 5xFADPrnp^{+}/$^{+}$ mice exhibited a significantly higher Aβ-plaque load compared to 5xFADPrnp^{-}/$^{-}$ (*$p = 0.04$). No statistically significant differences were observed in Aβ-plaque load across other brain regions.

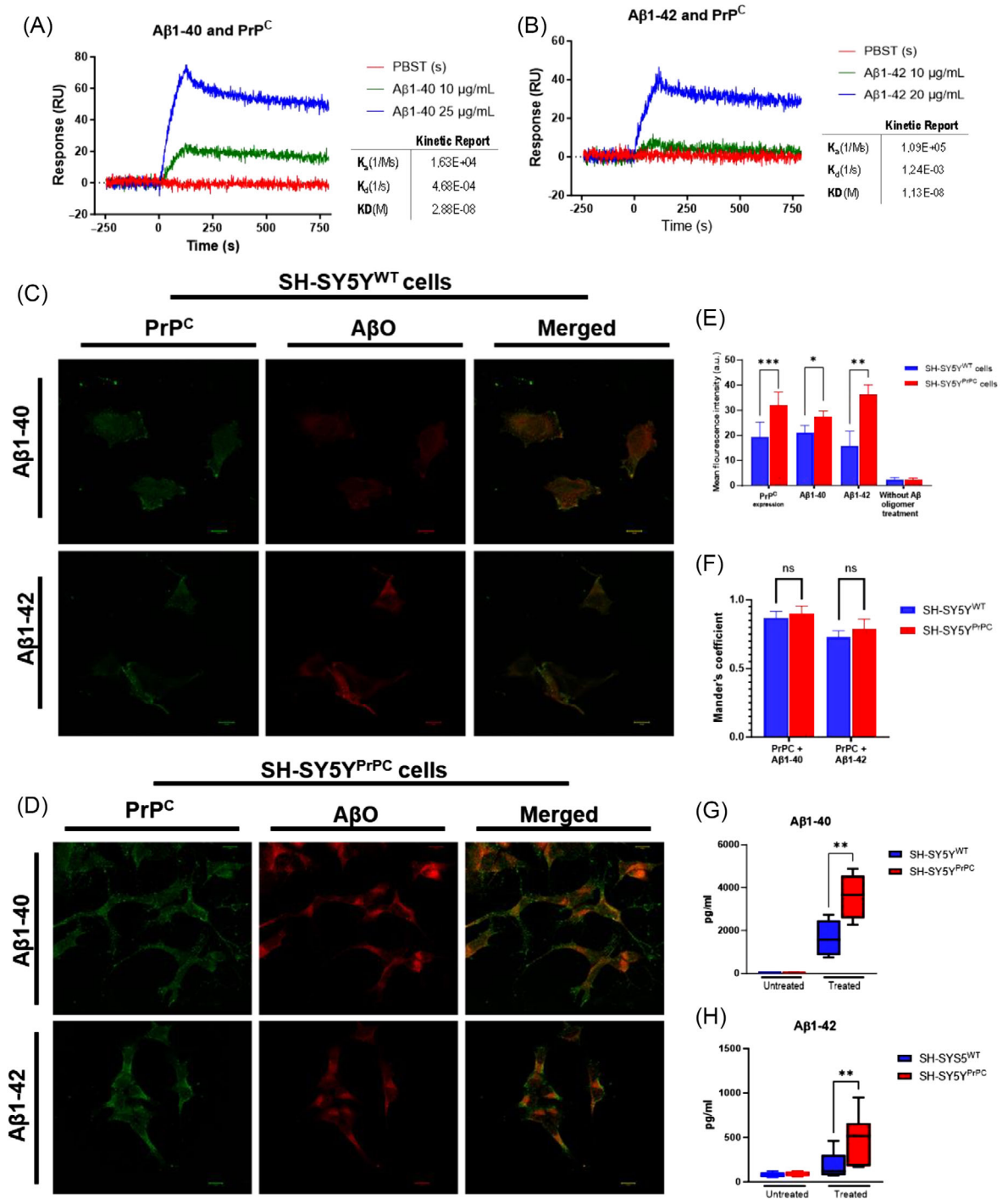

FIGURE 5 Interaction between PrP^C and Aβ peptides and their quantification in SH-SY5Y^{WT} and SH-SY5Y^{PrPC} cells. (A, B) SPR sensorgram analysis shows binding affinity between PrP^C and Aβ1-40 (KD = 2.88E-08 M) and Aβ1-42 (KD = 1.13E-08 M) binding. (C, D) Double immunostaining using SAF32 for PrP^C (green) and anti-Aβ antibody against Aβ1-40/Aβ1-42 oligomers (red) in SH-SY5Y^{WT} and SH-SY5Y^{PrPC} cells. Colocalization is represented by yellow in merged images (scale bars: 10 µm). (E) Mean fluorescence intensity analysis of PrP^C, Aβ1-40, and Aβ1-42 levels in SH-SY5Y^{WT} and SH-SY5Y^{PrPC} cells ($n = 20$) demonstrated significantly higher levels of Aβ1-40 (*$p < .05$) and Aβ1-42 (**$p < .01$) fluorescence intensity in SH-SY5Y^{PrPC} compared to SH-SY5Y^{WT} cells. (F) Mander's coefficient analysis revealed that similar colocalization degrees between PrP^C and Aβ1-40/Aβ1-42 were observed in SH-SY5Y^{WT} and SH-SY5Y^{PrPC} cells. (G, H) Quantification of Aβ1-40 and Aβ1-42 in treated and untreated SH-SY5Y^{WT} and SH-SY5Y^{PrPC} cells ($n = 20$) via ELISAs. Treated cells demonstrated a significant increase in both Aβ1-40 and Aβ1-42 levels compared to untreated cells. Furthermore, SH-SY5Y^{PrPC} cells exhibited significantly higher levels of Aβ1-40 ($p < .01$) and Aβ1-42 ($p < .01$) than SH-SY5Y^{WT}.

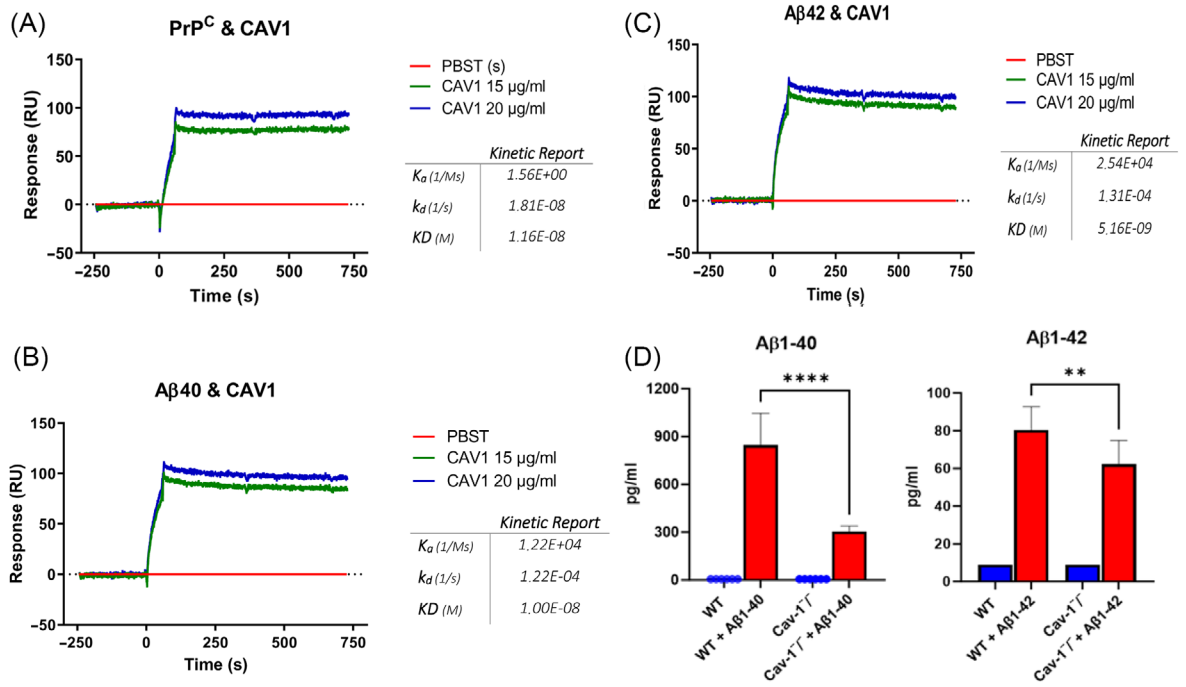

FIGURE 6 Interaction of PrP^C with Cav-1 and Aβ. (A, B) SPR sensorgrams depict binding affinity experiments between Cav-1 and Aβ1-40 and between Cav-1 and Aβ1-42, with equilibrium dissociation constants of 1.14E-08 and 1.30E-08, respectively. (C) The SPR sensorgram of Cav-1 and PrP^C illustrates a binding response with an equilibrium dissociation constant of 1.41E-08. (D) Aβ levels in WT and Cav-1 KO primary neurons were analyzed using ELISA. Quantification of Aβ1-40 revealed a significant decrease in Cav-1 KO neurons compared to WT neurons (****$p < .0001$). Statistical analyses of Aβ1-42 levels showed a significant decrease in Cav-1 KO neurons compared to WT neurons (**$p = .0017$) ($n = 12$).

mice expressing PrP^C compared to PrP^C-lacking mice.[38] We employed advanced imaging techniques to explore the distribution and the load of Aβ-plaque in a 3D context, allowing for precise location and comprehensive quantitative assessment across the entire brain.

4.3 | Interaction between PrP^C and Aβ peptides increases intracellular uptake of Aβ

SPR analyses revealed PrP^C's stable, direct interaction with Aβ1-40 and Aβ1-42. PrP^C showed a stronger binding affinity to Aβ1-42 (KD = 1.13E-08 M) than to Aβ1-40 (KD = 2.88E-08 M). These distinctions may have functional implications, given Aβ1-42's higher neurotoxicity,[39] suggesting PrP^C is a significant contributor to neurotoxicity. Our findings align with research supporting PrP^C as a high-affinity receptor for Aβo, corroborated by various methods such as co-immunoprecipitation, SPR (Aβ42 KD = 7.1E-08 M), and immunohistochemistry.[26,40–44] These studies primarily concentrated on PrP^C-Aβ1-42 interaction, but we extended our investigation to include Aβ1-40, exploring whether both Aβ1-40 and Aβ1-42 shared PrP^C as a receptor, and to determine their binding characteristics, shedding light on their similarities and mechanisms in AD pathology.

To explore PrP^C–Aβo interactions, SH-SY5Y^{WT} (low PrP^C expression) and stable transfected SH-SY5Y^{PrPC} (~five-fold higher PrP^C expression) were treated with Aβ1-40 and Aβ1-42 oligomers. PrP^C-overexpressing cells exhibited increased Aβ1-40 and Aβ1-42 levels compared to cells with normal PrP^C expression. Colocalization analyses showed consistent overlap of PrP^C–Aβo, indicating a high-affinity and specific PrP^C–Aβo, regardless of PrP^C expression levels. A study using hippocampal neurons and COS-7 cell line (derived from the CV-1 cell line with defective mutant of SV40) found PrP^C and Aβ1-42 oligomer interaction through immunostaining.[45] We provided a more comprehensive examination of PrP^C–Aβo interaction, incorporating distinct PrP^C expression cell lines and colocalization, including Aβ1-40, confirming the consistency of PrP^C–Aβo binding.

To gain insight into PrP^C–Aβ oligomer binding and potential uptake, Aβ1-40 and Aβ1-42 levels in the cell lysates were quantified via ELISA. PrP^C-overexpressing cells exhibited significantly higher Aβ levels (>200%) than control cells. Our findings align with previous research showing PrP^C and Aβ1-42 co-internalize in the SH-SY5Y cell line, detected by colocalization with subcellular markers and dot-blot.[46–48] Our quantitative approach, and the inclusion of Aβ1-40, supports PrP^C's general role in facilitating Aβ internalization, suggesting its involvement in intracellular Aβ accumulation and cell-to-cell spread. Intracellular Aβ accumulation precedes extracellular plaque formation in patients with Down syndrome.[7] In addition, in individuals with mild cognitive impairment (MCI), intraneural Aβ immunoreactivity has been observed in brain regions prone to early AD pathology, such as the hippocampus and entorhinal cortex.[49] Intracellular accumulation

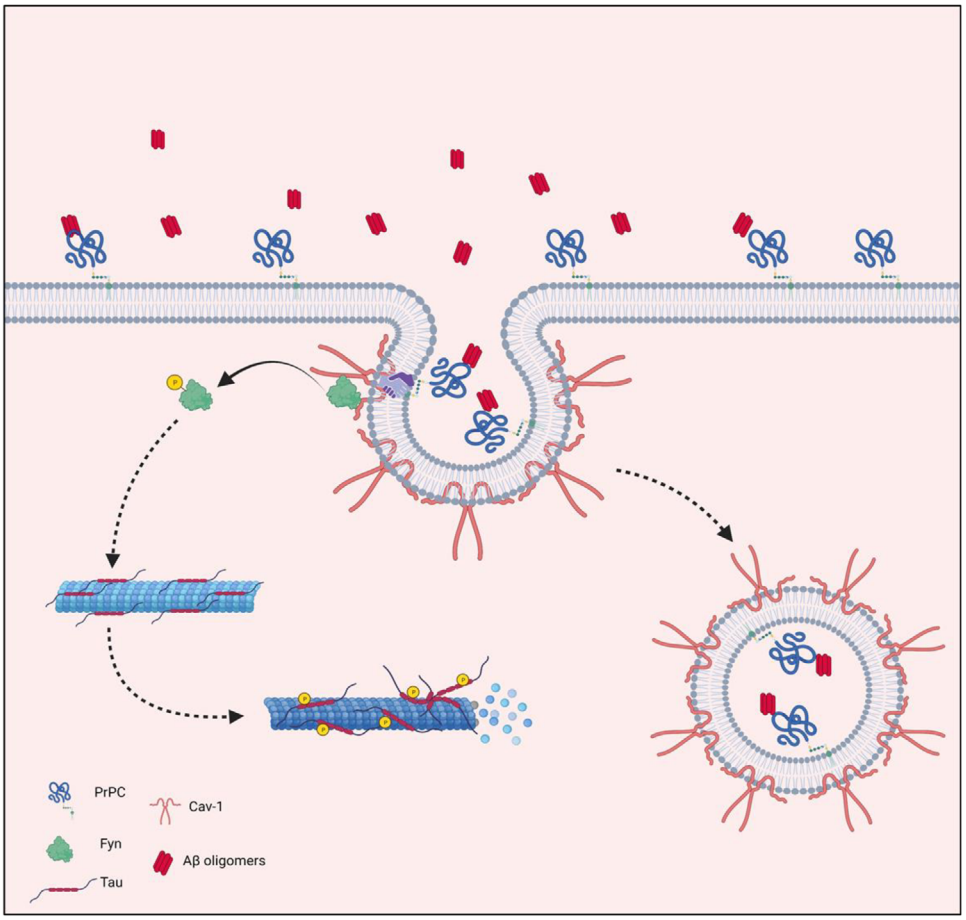

FIGURE 7 Schematic model of PrP^C and Cav-1/caveolae-dependent internalization of Aβo. Binding of extracellular Aβo on PrP^C activates a Cav-1/caveolae-dependent uptake mechanism potentially via activation of Fyn kinase. Fyn activation might trigger the excessive phosphorylation of tau protein, causing its detachment from microtubules. In addition, PrP^C–Aβo complexes potentially undergo internalization facilitated by PrP^C's interaction with Cav-1. This internalization mechanism could potentially elevate the intracellular Aβo levels and result in an increase of cellular stress and a disturbance of cellular homeostasis.

of Aβ it is believed to play an early role in AD pathogenesis.[49–51] This supports PrP^C as a potential target in AD therapeutics.

4.4 | Caveolin-1 expression modulates internalization of Aβ

PrP^C is enriched in caveolae or caveolae-like domains, participating in Fyn recruitment for signaling transduction.[52,53] Elevated Cav-1 levels were confirmed in AD patients' brains, supporting Cav-1's role in AD.[54] Therefore, we employed SPR to explore Cav-1's interaction with PrP^C, Aβ1-40, and Aβ1-42. Our study revealed a direct Cav-1–PrP^C interaction (KD = 1.41E-08 M), along with Cav-1–Aβ1-40 (KD = 1.14E-08 M) and Cav-1–Aβ1-42 (KD = 1.30E-08 M) interactions. One study found colocalization of PrP^C and Cav-1, along with an interaction between PrP^C's octa repeat region and Cav-1.[55] Interestingly, we observed a direct interaction between Cav-1 and Aβ1-40 and Aβ1-42. Previous studies reported Cav-1 interactions with APP C-terminal and its role in regulating APP cleavage by gamma secretase.[56]

To investigate Cav-1 KO's impact on Aβ internalization, primary cortical neurons from WT and Cav-1 KO mice were treated with Aβ1-40 and Aβ1-42 oligomers. The results revealed a substantial reduction of intracellular Aβ1-40 (approximately 65%) and Aβ1-42 (around 25%) in Cav-1 KO neurons compared to WT, indicating Cav-1's influence on Aβ internalization. This novel role of Cav-1 and caveolae in Aβ uptake provides new insights into potential AD molecular mechanisms. Although limited literature exists on Cav-1–PrP^C interaction, it has been reported that PrP^C binding to Cav-1 facilitates PrP^C internalization.[53,57,58] A link between PrP^C and Cav-1 was described in prostate and colon cancer, where they colocalize in MDST8 cells.[59] PrP^C-overexpressing LoVo cells upregulated Cav-1 mRNA, while PrP^C KO MDST8 cells reduced Cav-1 mRNA, suggesting an association between both proteins at transcriptomic and proteomic levels.[53,57–59] Studies hypothesized that PrP^C–Aβ binding and Cav-1 interaction activate Fyn, leading to tau hyperphosphorylation.[55,60] Considering our data and the existing literature, we hypothesize that, besides Fyn activation, PrP^C, when bound to Aβ, internalizes via caveolae mediated by Cav-1, increasing intracellular amounts of Aβ (Figure 7), which may

result in intracellular dysfunctions, such as cellular stress and apoptosis. This novel pathophysiological mechanism may further explain PrP^C's toxic role in AD.

In summary, our research underscores the crucial roles of PrP^C and Cav-1 in the complex processes of Aβ-mediated AD pathophysiology.

ACKNOWLEDGMENTS

We gratefully acknowledge Dr. Wiebke Möbius for her valuable contribution in providing electron microscopy images, which greatly enhanced the quality and scope of this research. This work was supported in part by Alzheimer Forschung Initiative (AFI, projects 12851 and 20026 to MS). Funding sources played no role in the design and conduct of the studies, data analyses, preparation of the manuscript, and the decision to submit the manuscript for publication.

Open access funding enabled and organized by Projekt DEAL.

CONFLICT OF INTEREST STATEMENT

The authors declare no conflicts of interest. Author disclosures are available in the supporting information.

CONSENT STATEMENT

Not necessary.

REFERENCES

1. World Health Organization. Dementia 2017. (accessed May 6, 2019). https://www.who.int/news-room/fact-sheets/detail/dementia
2. Crews L, Masliah E. Molecular mechanisms of neurodegeneration in Alzheimer's disease. *Hum Mol Genet*. 2010;19:R12-R20. doi:10.1093/hmg/ddq160
3. Kametani F, Hasegawa M. Reconsideration of amyloid hypothesis and tau hypothesis in Alzheimer's disease. *Front Neurosci*. 2018;12:25. doi:10.3389/fnins.2018.00025
4. Magalingam KB, Radhakrishnan A, Ping NS, Haleagrahara N. Current concepts of neurodegenerative mechanisms in Alzheimer's disease. *Biomed Res Int*. 2018;2018:1-12. doi:10.1155/2018/3740461
5. Oakley H, Cole SL, Logan S, et al. Intraneuronal β-amyloid aggregates, neurodegeneration, and neuron loss in transgenic mice with five familial Alzheimer's disease mutations: potential factors in amyloid plaque formation. *J Neurosci Res*. 2006;26:10129-10140. doi:10.1523/JNEUROSCI.1202-06.2006
6. Stokin GB, Lillo C, Falzone TL, et al. Axonopathy and transport deficits early in the pathogenesis of Alzheimer's disease. *Science*. 2005;307:1282-1288. doi:10.1126/science.1105681
7. Gyure KA, Durham R, Stewart WF, Smialek JE, Troncoso JC. Intraneuronal abeta-amyloid precedes development of amyloid plaques in Down syndrome. *Arch Pathol Lab Med*. 2001;125:489-492. doi:10.5858/2001-125-0489-IAAPDO
8. Mucke L, Selkoe DJ. Neurotoxicity of amyloid β-protein: synaptic and network dysfunction. *Cold Spring Harb Perspect Med*. 2012;2:a006338. doi:10.1101/cshperspect.a006338
9. Laurén J, Gimbel DA, Nygaard HB, Gilbert JW, Strittmatter SM. Cellular prion protein mediates impairment of synaptic plasticity by amyloid-beta oligomers. *Nature*. 2009;457:1128-1132. doi:10.1038/nature07761
10. Ferreira DG, Temido-Ferreira M, Miranda HV, et al. α-synuclein interacts with PrPC to induce cognitive impairment through mGluR5 and NMDAR2B. *Nat Neurosci*. 2017;20:1569-1579. doi:10.1038/NN.4648
11. Castle AR, Gill AC. Physiological functions of the cellular prion protein. *Front Mol Biosci*. 2017;4:19. doi:10.3389/fmolb.2017.00019
12. Büeler H, Fischer M, Lang Y, et al. Normal development and behaviour of mice lacking the neuronal cell-surface PrP protein. *Nature*. 1992;356:577-582. doi:10.1038/356577A0
13. Razani B, Engelman JA, Wang XB, et al. Caveolin-1 null mice are viable but show evidence of hyperproliferative and vascular abnormalities. *J Biol Chem*. 2001;276:38121-38138. doi:10.1074/JBC.M105408200
14. Fa M, Orozco IJ, Francis YI, Saeed F, Gong Y, Arancio O. Preparation of oligomeric β-amyloid1-42 and induction of synaptic plasticity impairment on hippocampal slices. *J Vis Exp*. 2010;41:1884. doi:10.3791/1884
15. Ryan DA, Narrow WC, Federoff HJ, Bowers WJ. An improved method for generating consistent soluble amyloid-beta oligomer preparations for in vitro neurotoxicity studies. *J Neurosci Methods*. 2010;190(2):171-179. doi:10.1016/j.jneumeth.2010.05.001
16. Da Silva Correia SM, Schmitz M, Fischer A, Hermann P, Zerr I. Role of different recombinant PrP substrates in the diagnostic accuracy of the CSF RT-QuIC assay in Creutzfeldt-Jakob disease. *Cell Tissue Res*. 2023;392:301-306. doi:10.1007/S00441-022-03715-9
17. Renier N, Wu Z, Simon DJ, Yang J, Ariel P, Tessier-Lavigne M. iDISCO: a simple, rapid method to immunolabel large tissue samples for volume imaging. *Cell*. 2014;159:896-910. doi:10.1016/J.CELL.2014.10.010
18. iDISCO+. iDISCO+ protocol Recommendations for sample handling 2016. (accessed July 16, 2023). https://idisco.info/
19. Yates SC, Groeneboom NE, Coello C, et al. QUINT: workflow for quantification and spatial analysis of features in histological images from rodent brain. *Front Neuroinform*. 2019;13:453735. doi:10.3389/FNINF.2019.00075/BIBTEX
20. Cissé M, Sanchez PE, Kim DH, Ho K, Yu GQ, Mucke L. Ablation of cellular prion protein does not ameliorate abnormal neural network activity or cognitive dysfunction in the J20 line of human amyloid precursor protein transgenic mice. *J Neurosci Res*. 2011;31:10427. doi:10.1523/JNEUROSCI.1459-11.2011
21. Westaway D, Jhamandas JH. The P's and Q's of cellular PrP-Aβ interactions. *Prion*. 2012;6:359-363. doi:10.4161/pri.20675
22. Gimbel DA, Nygaard HB, Coffey EE, et al. Memory impairment in transgenic Alzheimer mice requires cellular prion protein. *J Neurosci Res*. 2010;30:6367-6374. doi:10.1523/JNEUROSCI.0395-10.2010
23. Um JW, Nygaard HB, Heiss JK, et al. Alzheimer amyloid-β oligomer bound to post-synaptic prion protein activates fyn to impair neurons. *Nat Neurosci*. 2012;15:1227. doi:10.1038/NN.3178
24. Gunther EC, Smith LM, Kostylev MA, et al. Rescue of transgenic Alzheimer's pathophysiology by polymeric cellular prion protein antagonists. *Cell Rep*. 2019;26:145-158. doi:10.1016/j.celrep.2018.12.021. e8.
25. Chung E, Ji Y, Sun Y, Kascsak RJ, et al. Anti-PrPC monoclonal antibody infusion as a novel treatment for cognitive deficits in an alzheimer's disease model mouse. *BMC Neurosci*. 2010;11:130. doi:10.1186/1471-2202-11-130
26. Balducci C, Beeg M, Stravalaci M, et al. Synthetic amyloid-β oligomers impair long-term memory independently of cellular prion protein. *Proc Natl Acad Sci USA*. 2010;107:2295. doi:10.1073/PNAS.0911829107
27. Westerman MA, Cooper-Blacketer D, Mariash A, et al. The relationship between Aβ and memory in the Tg2576 mouse model of Alzheimer's disease. *J Neurosci Res*. 2002;22:1858-1867. doi:10.1523/JNEUROSCI.22-05-01858.2002
28. Trinchese F, Liu S, Battaglia F, Walter S, Mathews PM, Arancio O. Progressive age-related development of Alzheimer-like pathology in APP/PS1 mice. *Ann Neurol*. 2004;55:801-814. doi:10.1002/ana.20101
29. Foley AM, Ammar ZM, Lee RH, Mitchell CS. Systematic review of the relationship between amyloid-β levels and measures of transgenic mouse cognitive deficit in Alzheimer's disease. *J Alzheimer's Dis*. 2015;44:787-795. doi:10.3233/JAD-142208
30. Hardy J, Selkoe DJ. The amyloid hypothesis of Alzheimer's disease: progress and problems on the road to therapeutics. *Science (1979)*. 2002;297:353-356. doi:10.1126/science.1072994

31. Bloom GS. Amyloid-β and tau: the trigger and bullet in alzheimer disease pathogenesis. *JAMA Neurol*. 2014;71:505-508. doi:10.1001/JAMANEUROL.2013.5847
32. Schröder H, Moser N, Huggenberger S. *The mouse olfactory system. Neuroanatomy of the mouse*. Springer International Publishing; 2020:319-331. doi:10.1007/978-3-030-19898-5_14
33. Schröder H, Moser N, Huggenberger S. *The mouse hippocampus. Neuroanatomy of the mouse*. Springer International Publishing; 2020:267-288. doi:10.1007/978-3-030-19898-5_11
34. Schröder H, Moser N, Huggenberger S. *The mouse hypothalamus. Neuroanatomy of the mouse*. Springer International Publishing; 2020:205-230. doi:10.1007/978-3-030-19898-5_9
35. Schröder H, Moser N, Huggenberger S. *The mouse thalamus. Neuroanatomy of the mouse*. Springer International Publishing; 2020:171-203. doi:10.1007/978-3-030-19898-5_8
36. Schröder H, Moser N, Huggenberger S. *The mouse cerebral cortex. Neuroanatomy of the mouse*. Springer International Publishing; 2020:231-265. doi:10.1007/978-3-030-19898-5_10
37. Schwarze-Eicker K, Keyvani K, Görtz N, Westaway D, Sachser N, Paulus W. Prion protein (PrPc) promotes β-amyloid plaque formation. *Neurobiol Aging*. 2005;26:1177-1182. doi:10.1016/j.neurobiolaging.2004.10.004
38. Qin K, Zhao L, Gregory C, Solanki A, Mastrianni JA. "Dual Disease" TgAD/GSS mice exhibit enhanced Alzheimer's disease pathology and reveal PrPC-dependent secretion of Aβ. *Sci Rep*. 2019;9:8524. doi:10.1038/s41598-019-44317-w
39. Selkoe DJ. Alzheimer's disease: genes, proteins, and therapy. *Physiol Rev*. 2001;81:741-766. doi:10.1152/PHYSREV.2001.81.2.741
40. Smith LM, Kostylev MA, Lee S, Strittmatter SM. Systematic and standardized comparison of reported amyloid-β receptors for sufficiency, affinity, and Alzheimer's disease relevance. *J Biol Chem*. 2019;294:6042-6053. doi:10.1074/JBC.RA118.006252
41. Freir DB, Nicoll AJ, Klyubin I, et al. Interaction between prion protein and toxic amyloid β assemblies can be therapeutically targeted at multiple sites. *Nat Commun*. 2011;2:336. doi:10.1038/NCOMMS1341
42. Kessels HW, Nguyen LN, Nabavi S, Malinow R. The prion protein as a receptor for amyloid-β. *Nature*. 2010;466:E3. doi:10.1038/NATURE09217
43. Laurén J, Gimbel DA, Nygaard HB, Gilbert JW, Strittmatter SM. Cellular prion protein mediates impairment of synaptic plasticity by amyloid-β oligomers. *Nature*. 2009;457:1128. doi:10.1038/NATURE07761
44. Chen S, Yadav SP, Surewicz WK. Interaction between human prion protein and amyloid-β (Aβ) oligomers. *J Biol Chem*. 2010;285:26377-26383. doi:10.1074/jbc.M110.145516
45. Laurén J, Gimbel DA, Nygaard HB, Gilbert JW, Strittmatter SM. Cellular prion protein mediates impairment of synaptic plasticity by amyloid-β oligomers. *Nature*. 2009;457:1128-1132. doi:10.1038/nature07761
46. Rushworth JV, Griffiths HH, Watt NT, Hooper NM. Prion protein-mediated toxicity of amyloid-β oligomers requires lipid rafts and the transmembrane LRP1. *J Biol Chem*. 2013;288:8935-8951. doi:10.1074/jbc.M112.400358
47. Boroujeni ER, Hosseini SM, Fani G, Cecchi C, Chiti F. Soluble prion peptide 107-120 protects neuroblastoma SH-SY5Y cells against oligomers associated with Alzheimer's disease. *Int J Mol Sci*. 2020;21:1-21. doi:10.3390/IJMS21197273
48. Foley AR, Roseman GP, Chan K, et al. Evidence for aggregation-independent, PrPC-mediated Aβ cellular internalization. *Proc Natl Acad Sci USA*. 2020;117:28625-28631. doi:10.1073/PNAS.2009238117/-/DCSUPPLEMENTAL
49. Gouras GK, Tsai J, Naslund J, et al. Intraneuronal Aβ42 accumulation in human brain. *Am J Pathol*. 2000;156:15. doi:10.1016/S0002-9440(10)64700-1
50. Oddo S, Caccamo A, Shepherd JD, et al. Triple-transgenic model of Alzheimer's Disease with plaques and tangles: intracellular Aβ and synaptic dysfunction. *Neuron*. 2003;39:409-421. doi:10.1016/S0896-6273(03)00434-3
51. LaFerla FM, Green KN, Oddo S. Intracellular amyloid-beta in Alzheimer's disease. *Nat Rev Neurosci*. 2007;8:499-509. doi:10.1038/NRN2168
52. Harmey JH, Doyle D, Brown V, Rogers MS. The cellular isoform of the prion protein, PrPc, is associated with caveolae in mouse neuroblastoma (N2a) cells. *Biochem Biophys Res Commun*. 1995;210:753-759. doi:10.1006/BBRC.1995.1723
53. Mouillet-Richard S, Ermonval M, Chebassier C, et al. Signal transduction through prion protein. *Science (1979)*. 2000;289:1925-1928. doi:10.1126/science.289.5486.1925
54. Gaudreault SB, Dea D, Poirier J. Increased caveolin-1 expression in Alzheimer's disease brain. *Neurobiol Aging*. 2004;25:753-759. doi:10.1016/J.NEUROBIOLAGING.2003.07.004
55. Shi Q, Jing Y-Y, Wang S-B, et al. PrP octarepeats region determined the interaction with caveolin-1 and phosphorylation of caveolin-1 and Fyn. *Med Microbiol Immunol*. 2013;202:215-227. doi:10.1007/s00430-012-0284-8
56. Ikezu T, Trapp BD, Song KS, Schlegel A, Lisanti MP, Okamoto T. Caveolae, plasma membrane microdomains for alpha-secretase-mediated processing of the amyloid precursor protein. *J Biol Chem*. 1998;273:10485-10495. doi:10.1074/JBC.273.17.10485
57. Peters PJ, Mironov A, Peretz D, et al. Trafficking of prion proteins through a caveolae-mediated endosomal pathway. *J Cell Biol*. 2003;162:703-717. doi:10.1083/JCB.200304140
58. Toni M, Spisni E, Griffoni C, et al. Cellular prion protein and caveolin-1 interaction in a neuronal cell line precedes Fyn/Erk 1/2 signal transduction. *J Biomed Biotechnol*. 2006;2006(5):69469. doi:10.1155/JBB/2006/69469
59. Mouillet-Richard S, Martin-Lannerée S, Le Corre D, et al. A proof of concept for targeting the PrPC—Amyloid β peptide interaction in basal prostate cancer and mesenchymal colon cancer. *Oncogene*. 2022;41:4397-4404. doi:10.1038/s41388-022-02430-7
60. Larson M, Sherman MA, Amar F, et al. The complex PrP ^{c} -Fyn couples human oligomeric Aβ with pathological tau changes in Alzheimer's disease. *J Neurosci Res*. 2012;32:16857-16871. doi:10.1523/JNEUROSCI.1858-12.2012

SUPPORTING INFORMATION

Additional supporting information can be found online in the Supporting Information section at the end of this article.

How to cite this article: da Silva Correia A, Schmitz M, Fischer A-L, et al. Cellular prion protein acts as mediator of amyloid beta uptake by caveolin-1 causing cellular dysfunctions in vitro and in vivo. *Alzheimer's Dement*. 2024;20:6776–6792. https://doi.org/10.1002/alz.14120